© 2016. Published by The Company of Biologists Ltd | Journal of Cell Science (2016) 129, 843-853 doi:10.1242/jcs.180356

RESEARCH ARTICLE

Reverse overshot water-wheel retroendocytosis of apotransferrin extrudes cellular iron

Navdeep Sheokand[1], Himanshu Malhotra[1], Anoop Singh Chauhan[1], Manoj Kumar[1], Surbhi Chaudhary[1], Anil Patidar[1], Vishant Mahendra Boradia[2], Chaaya Iyengar Raje[2] and Manoj Raje[1,*]

ABSTRACT

Iron (Fe), a vital micronutrient for all organisms, must be managed judiciously because both deficiency or excess can trigger severe pathology. Although cellular Fe import is well understood, its export is thought to be limited to transmembrane extrusion through ferroportin (also known as Slc40a1), the only known mammalian Fe exporter. Utilizing primary cells and cell lines (including those with no discernible expression of ferroportin on their surface), we demonstrate that upon Fe loading, the multifunctional enzyme glyceraldehyde-3-phosphate dehydrogenase (GAPDH), which is recruited to the cell surface, 'treadmills' apotransferrin in and out of the cell. Kinetic analysis utilizing labeled ligand, GAPDH-knockdown cells, ^{55}Fe-labeled cells and pharmacological inhibitors of endocytosis confirmed GAPDH-dependent apotransferrin internalization as a prerequisite for cellular Fe export. These studies define an unusual rapid recycling process of retroendocytosis for cellular Fe extrusion, a process mirroring receptor mediated internalization that has never before been considered for maintenance of cellular cationic homeostasis. Modulation of this unusual pathway could provide insights for management of Fe overload disorders.

KEY WORDS: Glyceraldehyde-3-phosphate dehydrogenase, GAPDH, Apotransferrin, Moonlighting protein, Iron, Retroendocytosis, Microscopy, Protein trafficking

INTRODUCTION

A fundamental requirement for all life processes from the cellular to societal level is the ability to maintain a physiological balance of nutrients. This involves the establishment of regulated mechanisms for their intake (to overcome deficiency) coupled with moderated extrusion of any excess material (to prevent deleterious accumulation). Among the transition metal ions, iron ions (Fe; for which there are several oxidation states, most commonly Fe^{2+} and Fe^{3+}) are most abundantly present in biological systems and essential for all life. They play a crucial role in oxidative energy metabolism. Although Fe is indispensable for cells, an excess of intracellular Fe is also perilous as it produces highly reactive and destructive free radicals (Hentze et al., 2004). To maintain homeostasis, nature has evolved a delicately balanced system for its absorption, transport, storage and recycling. A high serum concentration of unsaturated Fe-carrier protein apotransferrin keeps a rein on free Fe to avoid any toxic effects. Although cellular Fe-uptake pathways through receptor-mediated transferrin uptake are very well characterized, export of this double-edged nutrient from cells is still poorly explored. Currently, our knowledge regarding its exit is restricted to the perception that intracellular Fe is pumped out through the membrane transporter ferroportin (also known as IREG1, MTP1 and Slc40a1), the only known Fe exporter in mammals (De Domenico et al., 2007; Donovan et al., 2006; Le Gac et al., 2013; Ward and Kaplan, 2012). Expressed primarily on the basolateral surface of duodenal enterocytes, ferroportin is also present on the surface of tissue macrophages and hepatocytes. This molecular pump extrudes cellular Fe across the plasma membrane (Canonne-Hergaux et al., 2006; McKie et al., 2000; Ramey et al., 2010). Fe loading enhances the localization of ferroportin onto the plasma membrane of macrophages in a manner that is negatively regulated by hepcidin (Delaby et al., 2005; Nemeth et al., 2004). However, considerable ambiguity still remains as to how excess Fe is cleared from all those cells that do not express ferroportin on their surface, or where cell surface ferroportin expression is refractory to Fe levels. Although intracellular vesicular trafficking of apotransferrin has been suspected to contribute to the export of Fe from cells (Linder, 2013; Ma et al., 2002; Moriya and Linder, 2006; Zhang et al., 2011), to date, no definitive receptor or any pathway for trafficking of apotransferrin has been found, and the accepted view remains that excess cellular Fe is pumped out across the plasma membrane by ferroportin (Ross et al., 2012).

Recently, utilizing cell culture as well as animal models of Fe overload, we have demonstrated that Fe-loaded macrophages and hepatocytes (two of the principal cell types involved in recycling and storage of Fe) enhance the expression of a distinct post-translationally modified isoform of GAPDH in close proximity to ferroportin on their surface. This isoform of GAPDH captures apotransferrin with high affinity and enhances cellular Fe export. The model proposed for this process involves Fe extrusion from cells through the classic cell surface ferroportin pump, followed by rapid chelation of the externalized Fe into apotransferrin (Sheokand et al., 2014). These findings still cannot explain as to how the vast majority of cells that lack ferroportin on their surface are able to extrude excess of the metal ions (D'Anna et al., 2009; Donovan et al., 2005), and the possibility that GAPDH utilizes an alternative method to remove Fe from cells in a surface-ferroportin-independent manner cannot be ruled out. In the current study, using different primary cell types and cell lines that lack surface ferroportin, we demonstrate that surface GAPDH recruited upon Fe accumulation is able to not only capture but to also internalize apotransferrin into cells to chelate Fe intracellularly. Subsequent retroendocytosis of the internalized protein brings about cellular Fe release. We also confirm the existence and operation of this pathway in cells such as macrophages, which also utilize surface ferroportin for this purpose.

RESULTS

To understand the mechanism of Fe extrusion from cells that lack surface ferroportin, we first investigated whether the phenomenon of Fe-dependent enhanced surface expression of GAPDH and

[1]Institute of Microbial Technology, CSIR, Sector 39A, Chandigarh 160036, India. [2]National Institute of Pharmaceutical Education & Research, Phase X, Sector 67, SAS Nagar, Punjab 160062, India.

*Author for correspondence (manoj@imtech.res.in)

Received 10 September 2015; Accepted 29 December 2015

Journal of Cell Science (2016) 129, 843-853 doi:10.1242/jcs.180356

corresponding increased apotransferrin capture is restricted only to macrophages and hepatocytes (that abundantly express ferroportin on their surface) or whether it is a more prevalent phenomenon. Studies revealed a correlated increase in surface GAPDH and apotransferrin capture by disparate cells (Table 1). Analysis of ferroportin expression revealed that CHO-TRVb cells expressed a low level of the protein intracellularly, which remained unchanged even after Fe loading (Fig. 1A; Fig. S1A). Notably, no ferroportin expression was detected on the surface of control or Fe-treated CHO-TRVb cells (Fig. 1B; Fig. S1B). Mouse spleen lymphocytes, human lymphocytes and non-macrophage murine bone marrow cells also did not show any ferroportin on their surface under control or Fe-loaded conditions (Fig. S1C). By contrast, in agreement with earlier reports, macrophages from both spleen and bone marrow demonstrated Fe-dependent ferroportin expression on their membranes (Fig. S1C). A saturation binding assay revealed the presence of high-affinity apotransferrin-binding sites (K_d=1.55 nM) on the surface of CHO-TRVb cells (Fig. 1C). This matches well with our earlier reported value of 1.1 nM for apotransferrin binding of GAPDH on J774 cells, it is also similar to the K_d of 5.3 nM reported by us for the *in vitro* GAPDH–apotransferrin interaction (Sheokand et al., 2014). Co-immunoprecipitation analysis confirmed the interaction of apotransferrin with surface GAPDH (Fig. 1D). Our earlier work has also established the role of GAPDH in apotransferrin-facilitated Fe export from macrophages and hepatocytes (Sheokand et al., 2014), and here too we observed that knockdown of GAPDH (see Materials and Methods) significantly compromised the ability of Fe-loaded CHO-TRVb cells to export Fe in the presence of apotransferrin (Fig. 1E; Fig. S1D). The phenomenon of apotransferrin-mediated enhanced Fe export was also confirmed in rat spleen lymphocytes, human lymphocytes and non-macrophage rat bone marrow cells, all of which do not have ferroportin on their membrane (Fig. 1F; Fig. S1C). This GAPDH-dependent capability of apotransferrin to facilitate removal of Fe from cells even in the absence of surface ferroportin suggests the existence of an alternative mechanism for Fe export where Fe is not directly pumped out of cells by ferroportin across the plasma membrane.

To explain the mechanism for this surface ferroportin-independent Fe exit, we explored the possibility of GAPDH-mediated apotransferrin trafficking into cells for sequestration and evacuation of intracellular Fe. This could involve a process akin to receptor-mediated trafficking of holotransferrin into cells for intracellular Fe delivery, followed by recycling of the residual apotransferrin along with receptor back to the cell surface, but instead operating in reverse. Such a form of retroendocytosis has previously been described for high-density lipoprotein (HDL) and apolipoprotein A-I endocytosis (followed by recycling and secretion) in diverse cell types (including macrophages), and has been linked to lipid intake and cholesterol efflux (Azuma et al., 2009; Pagler et al., 2006; Röhrl and Stangl, 2013). Fe-loaded J774, THP1 and CHO-TRVb cells all demonstrated a significant increase in internalization of radiolabeled apotransferrin, whereas GAPDH-knockdown THP1 and CHO-TRVb cells failed to increase apotransferrin uptake (Fig. 2A). Confocal microscopy analysis demonstrated the colocalization of GAPDH (that was initially resident on the cell surface) with apotransferrin within Fe-loaded cells (Fig. 2B; Fig. S2A). Immunoelectron microscopy analysis also revealed the presence of both proteins in endosomes of CHO-TRVb cells (Fig. 2Di,Dii). Co-immunoprecipitation of biotinylated apotransferrin with GAPDH from Fe-loaded CHO-TRVb and J774 cell endosomes (Fig. 2E), and an acceptor-photobleaching-based Förster resonance energy transfer (FRET) assay (Fig. 2F) confirmed the interaction between the two internalized proteins. The FRET efficiency measured was 27.79%±6.2 (mean±s.d.) (Fig. 2G).

Receptor-mediated endocytic processes are saturable and specific, also the involvement of any extracellular membrane protein would render the process sensitive to treatment of the cell surface with proteolytic enzymes (Steil et al., 1996). The dose-dependent apotransferrin uptake by Fe-loaded CHO-TRVb cells was found to be saturable (Fig. S2B), and incubation in the presence of excess unlabeled ligand inhibited ligand uptake (Fig. S2C), indicating the specific nature of the process. Finally, we also found that ligand uptake was significantly diminished when cells were pre-treated with the proteolytic enzyme pronase (Fig. S2D).

Treatment of cells with Dynasore® (a specific and potent inhibitor of endocytosis) not only decreased apotransferrin internalization but also inhibited the apotransferrin-mediated Fe export (Fig. 3A), whereas surface expression of ferroportin remained unchanged (Fig. 3B). This excludes the possibility of a decrease in Fe export occurring owing to any diminution in availability of ferroportin for transport of the ions across the plasma membrane. To further confirm that the process of apotransferrin internalization is crucial for cellular Fe export and also to investigate the nature of the endocytic process, this phenomenon was further investigated in CHO-TRVb cells utilizing a diverse panel of pharmacological inhibitors for endocytosis. Inhibitors of the lipid-raft-mediated endocytosis had no significant effect on apotransferrin internalization or Fe export. By contrast, pharmacological agents that compromise clathrin-pit-mediated endocytosis significantly inhibited apotransferrin internalization, along with export of Fe. Similar results of co-inhibition were observed with cytoskeleton-perturbing agents, phosphoinositide 3-kinase (PI3K) inhibition and ATP depletion, indicating the involvement of additional pathways and the energy-dependent nature of the process (Fig. 3C,D). The strong correlation observed between apotransferrin internalization and inhibition of Fe export confirmed the pre-requisite requirement of apotransferrin import for Fe export (Fig. 3E). Fe estimation by using atomic absorption spectrometry revealed that endosomes of Fe-loaded cells accumulated more Fe (12.16±1.27 ng/µg protein; mean±s.d.) as compared to control cells (6.54±2.1 ng/µg protein). Finally, we also observed that apotransferrin that had been imported into Fe-loaded cells chelated intracellular Fe and subsequently exited the cells along with the incorporated Fe (Fig. 3F).

Earlier work has reported the involvement of intracellular ferroportin in Fe trafficking between cytosol and an intracellular

Table 1. Effect of cellular Fe loading on GAPDH surface expression and apotransferrin binding

Cell type	Surface GAPDH	Apotransferrin binding
Human lymphocytes	4±0.28	2.46±0.16
Rat bone marrow cells	1.93±0.2	1.87±0.09
Rat spleen lymphocytes	1.72±0.1	1.43±0.09
CHO	1.94±0.15	1.76±0.1
CHO-TRVb	1.77±0.27	1.83±0.03
NS	2.28±0.15	1.83±0.09

The fold change in surface expression of GAPDH and apotransferrin binding upon Fe loading, as compared to control cells at 24 h, evaluated by flow cytometry. (Student's *t*-test, compared to control cells), $n=10^4$ cells in each case, all experiments repeated at least three times. Data are presented as fold change±s.d. The increase in apotransferrin capture correlates with the increase in GAPDH recruitment to the cell surface in all cases, Spearman correlation r=0.91.

Journal of Cell Science (2016) 129, 843-853 doi:10.1242/jcs.180356

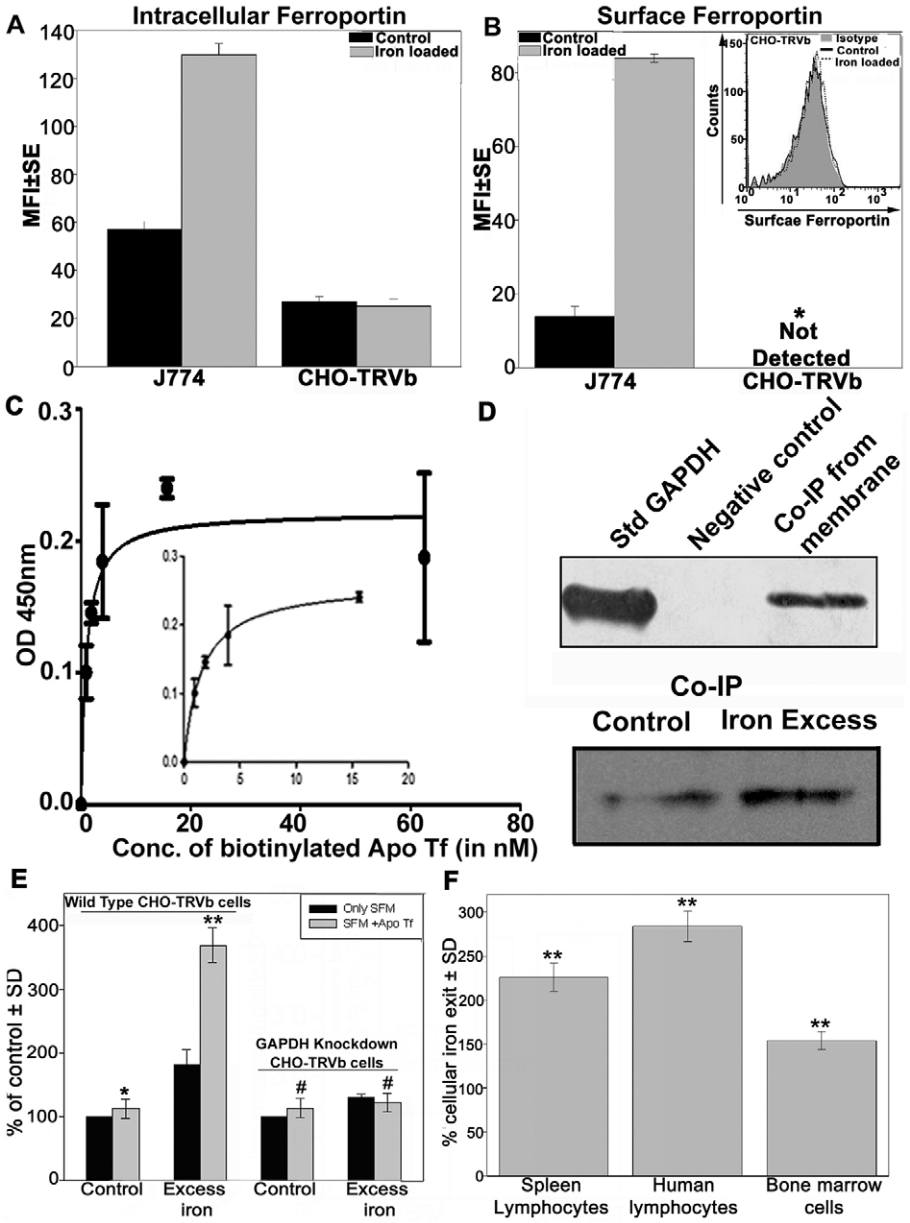

Fig. 1. Cells lacking surface ferroportin can also efflux Fe in an apotransferrin- and GAPDH-dependent manner. (A,B) Ferroportin expression in Fe-loaded J774 and CHO-TRVb cells. J774 and CHO-TRVb cells were treated with 100 µM $FeCl_3$, and intracellular (A) and surface (B) expression of ferroportin as compared to untreated controls was evaluated. CHO-TRVb cells were refractory to Fe, whereas J774 macrophages responded as reported previously and serve as a positive control here. A complete absence of any surface ferroportin in control or Fe-loaded CHO-TRVb cells was found (inset in B). Also see Fig. S1A–C. Data are presented as mean fluorescence intensity (MFI)±s.e.m., $P<0.0001$, $^{*}P>0.05$, $n=10^4$ cells, experiment repeated three times. (C) Concentration-dependent binding of apotransferrin on the surface of Fe-loaded CHO-TRVb cells. Bound ligand was detected with Streptavidin–HRP. Results are expressed as the concentration of apotransferrin (Apo Tf) versus the $OD_{450\ nm}$±s.d. The equilibrium dissociation constant was calculated by fitting data to nonlinear regression for one site specific saturable binding using GraphPad® software. (D) GAPDH and apotransferrin interaction on the surface of CHO-TRVb cells is revealed by co-immunoprecipitation (Co-IP). Fe-loaded CHO-TRVb cells were incubated with biotinylated apotransferrin to allow surface capture, and the purified membrane fraction was used for co-immunoprecipitation with Streptavidin magna beads. Interaction with GAPDH was confirmed by western blot using a monoclonal anti-GAPDH antibody. A control was performed wherein incubation of cells with biotinylated apotransferrin was omitted (upper panel). Western blot demonstrating GAPDH apotransferrin interaction on the membrane of control and Fe-loaded cells (lower panel). Std, standard rabbit muscle GAPDH. (E,F) Apotransferrin-facilitated Fe export from cells that lack surface ferroportin is GAPDH dependent. Cells that do not express ferroportin on their surface (CHO-TRVb, rat bone marrow cells, rat spleen lymphocytes and human lymphocytes) were subjected to an Fe overload through incubation in 100 µM $FeCl_3$ spiked with 500 nM of radioactive Fe for 12 h, whereas control cells were left untreated. Subsequent incubation with apotransferrin significantly facilitated Fe export from wild-type but not GAPDH-knockdown CHO-TRVb cells. $^{*}P<0.05$, $^{**}P<0.0005$, $^{\#}P>0.05$, $n=4$ replicates (E), see also Fig. S1D. Apotransferrin also enhances Fe removal from primary rat spleen and human lymphocytes as well as rat bone marrow cells, $^{**}P<0.001$, $n=4$ replicates (F). Data are presented as the percentage CPM of control ±s.d., where each experiment was repeated three times. All *P*-values were determined using Student's *t*-test, unless indicated otherwise.

vesicular compartment, a process in which ferroportin or NRAMP-family Fe transporters could act as an Fe 'concentrator' for export from cells (Abboud and Haile, 2000; Canonne-Hergaux et al., 2006; Linder et al., 2006; Soe-Lin et al., 2009). We too observed the presence of ferroportin in apotransferrin-positive vesicles (Fig. S3), which could explain the accumulation of Fe in endosomes of

Journal of Cell Science

Journal of Cell Science (2016) 129, 843-853 doi:10.1242/jcs.180356

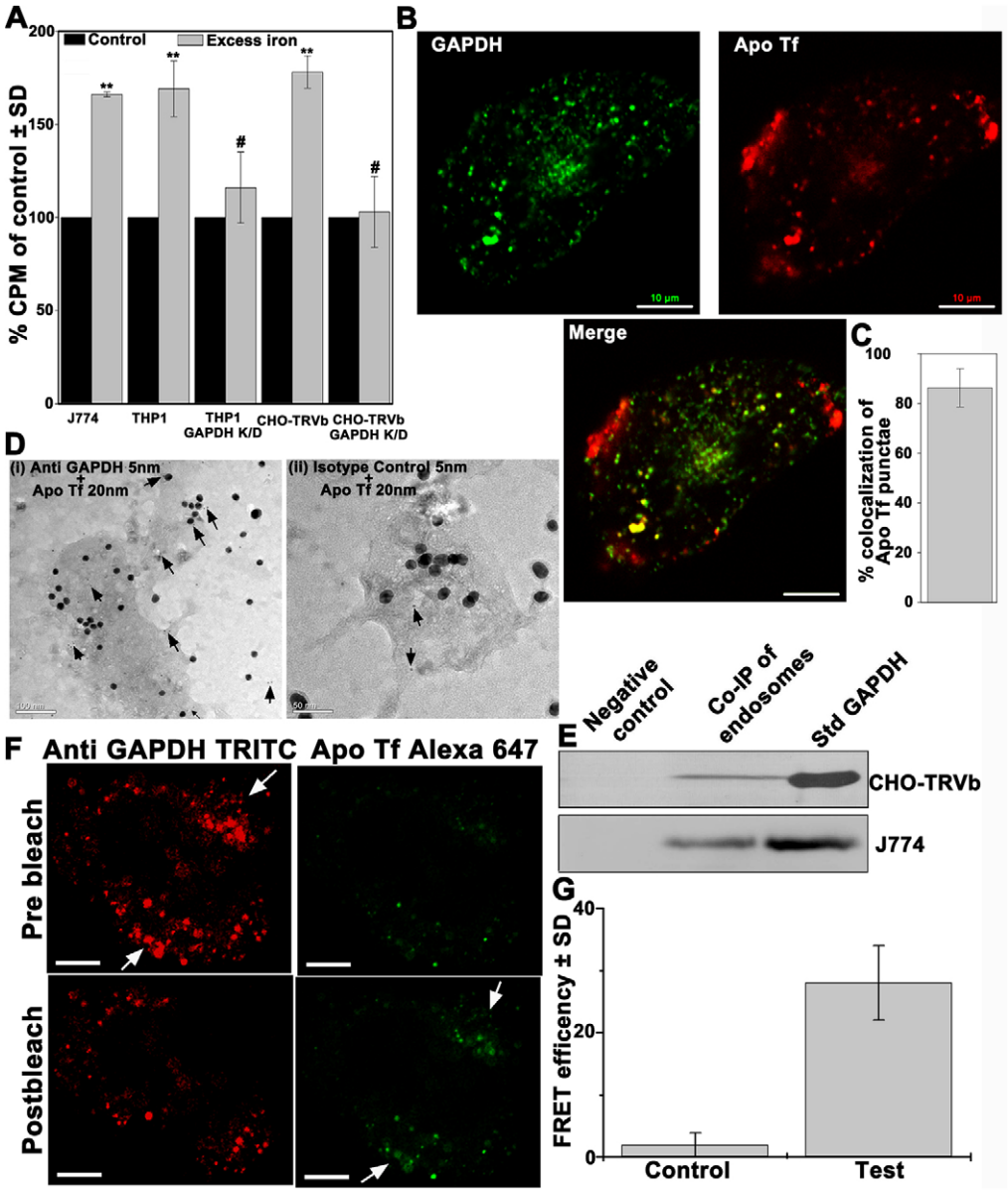

Fig. 2. Internalization of apotransferrin by Fe-loaded cells is a GAPDH-mediated process. (A) Cells were plated in a 24-well plate (2×10^5 cells/well) and loaded with Fe for 24 h. Controls, set in parallel, were maintained in normal medium. After treatment, cells were incubated with 20 µg apotransferrin ^{125}I at 37°C for 10 min and then treated with 0.1% pronase at 4°C for 10 min to remove any residual surface-bound ligand. Finally, cells were lysed and cell-associated radioactivity was measured. [I^{125}]Apotransferrin uptake is significantly enhanced in all Fe-loaded cells, except where knockdown of GAPDH had been performed (GAPDH KD). Data are presented as the percentage CPM of control±s.d., $^{**}P<0.0001$, $^{\#}P>0.05$, $n=4$ replicates. (B) The cell surface GAPDH–apotransferrin complex traffics into cells. Cells grown on glass coverslips were incubated with 1 µg of monoclonal anti-GAPDH antibody (Calbiochem) followed by rabbit anti-mouse FITC-conjugated antibody (Sigma-Aldrich) and 10 µg of apotransferrin–Alexa-Fluor-647 at 4°C and subsequently shifted to 37°C for 10 min to internalize surface-bound proteins. After fixation with paraformaldehyde, cells were imaged with a confocal microscope using 60× oil immersion objective and 1 airy unit aperture. Apo Tf, apotransferrin. Scale bars: 10 µm. (C) A large fraction of internalized apotransferrin colocalizes with GAPDH (86.27%±7.73, $n=10$ cells with a minimum 50 vesicles of apotransferrin per cell; mean±s.d.). (D) Co-internalization of apotransferrin and cell surface GAPDH into endosomes. GAPDH on the surface of Fe-loaded CHO-TRVb cells was tagged with an antibody against GAPDH (Sigma-Aldrich) (i) or isotype control (ii) followed by anti-rabbit IgG 5-nm-gold-conjugated antibody (arrows), simultaneously, cells were incubated with apotransferrin conjugated to 20-nm gold particles. (E) Co-immunoprecipitation (co-IP) of internalized apotransferrin and GAPDH. Fe-loaded CHO-TRVb or J774 cells were incubated with biotinylated apotransferrin at 37°C for 10 min before preparation of the endosomal fraction, which was subjected to co-immunoprecipitation using Streptavidin magna beads. Interaction between the two proteins was confirmed by western blotting using a monoclonal antibody against GAPDH. A control was run in parallel, in which incubation of cells with biotinylated apotransferrin was omitted. Std, standard rabbit muscle GAPDH. (F) Intracellular interaction between the two proteins visualized with FRET analysis. The FRET signal, which is represented by an increase (arrows) in donor intensity (monoclonal antibody against GAPDH detected with an anti-mouse IgG TRITC-conjugated antibody) upon bleaching of acceptor (apotransferrin–Alexa-Fluor-647). Scale bars: 10 µm. (G) FRET efficiency for control and test samples, $P<0.0001$, $n=25$ ROI (region of interest in different cells). See also Fig. S2. All *P*-values were determined using Student's *t*-test, unless indicated otherwise.

Fe-loaded cells. However, the involvement of other Fe transporters, such as DMT1, cannot be ruled out because DMT1 is known to colocalize intracellularly with apotransferrin (Leong and Lönnerdal, 2005; Ma et al., 2002), and a role for DMT1 in Fe secretion (Ludwiczek et al., 2007) and recycling (Soe-Lin et al., 2010) has been considered.

Journal of Cell Science (2016) 129, 843-853 doi:10.1242/jcs.180356

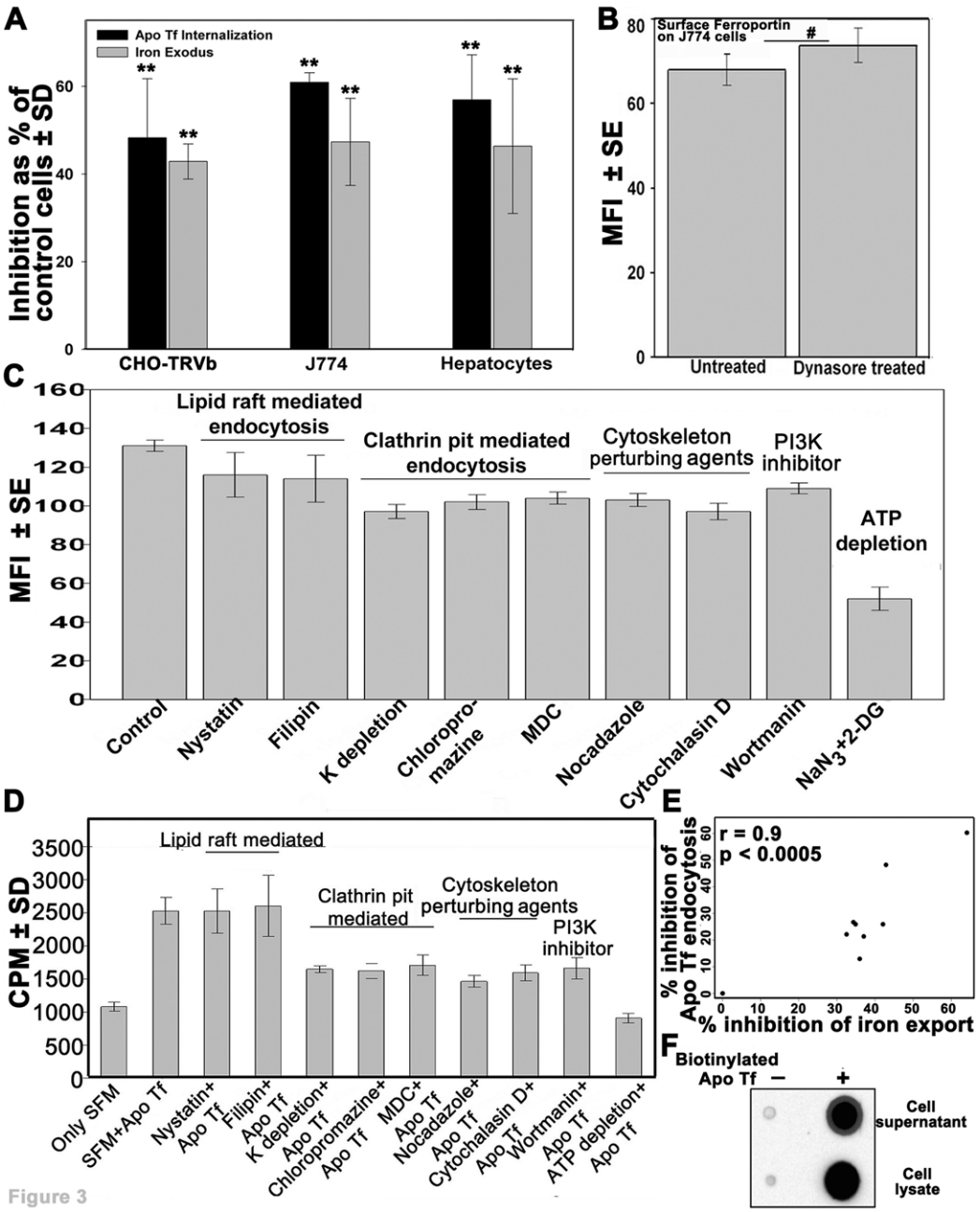

Figure 3

Fig. 3. Cellular Fe extrusion is coupled to apotransferrin internalization. (A) Cells were first Fe loaded by incubation in medium containing 100 µM $FeCl_3$+500 nM [^{55}Fe]Cl_3 for 12 h and then were pre-incubated with 80 µM Dynasore at 37°C for 10 min. In control samples, drug treatment was omitted. Subsequently, cells were assayed for internalization of apotransferrin–Alexa-Fluor-647 and Fe export. Prior treatment of cells with Dynasore® significantly inhibited both apotransferrin internalization (**P<0.0001, n=10^4 cells, experiment repeated three times) and apotransferrin-dependent Fe export (**P<0.0001, n=4 replicates). Data are presented as a percentage of that of Fe-loaded control cells±s.d. (B) Surface expression of ferroportin is not altered by Dynasore treatment. Data are presented as MFI±s.e.m. ($^{\#}P$>0.05, n=10^4 cells, experiment repeated three times). (C) Sensitivity of apotransferrin internalization to a diverse panel of endocytosis inhibitors. Fe-loaded CHO-TRVb cells were treated with a diverse panel of pharmacological inhibitors of endocytosis and then evaluated for the ability to internalize apotransferrin–Alexa-Fluor-647 over 10 min by using flow cytometry. Data are presented as MFI±s.e.m. P values were calculated in comparison to control cells where drug was omitted., P>0.05 (for blockers of lipid-raft-mediated endocytosis), P<0.0001 (for inhibitors of clathrin-pit-mediated endocytosis, cytoskeleton-perturbing agents, inhibition of PI3K by wortmanin and ATP depletion), n=10^4 cells in all cases, experiment repeated three times. (D) Fe export is also inhibited by the same agents that inhibit apotransferrin internalization. Data are presented as CPM±s.d., P<0.001 in all cases, except for inhibitors of lipid-raft-mediated endocytosis where P>0.05, n=4 replicates. (E) A strong correlation exists between the inhibition of cellular Fe exodus versus the inhibition of apotransferrin internalization, two-tailed Pearson correlation coefficient r=0.9, P<0.0005. (F) Intracellular Fe is sequestered into apotransferrin, which is released into the extracellular medium. Cells were first Fe loaded by incubation in medium containing 100 µM $FeCl_3$+500 nM [^{55}Fe]Cl_3 as above. Subsequently, the cells were incubated with 0.5 mg/ml of biotinylated apotransferrin, which was then allowed to recycle between the surface and cytosol for 1 h. Biotinylated apotransferrin was immunoprecipitated from the cell-free supernatant as well as cell lysate using Streptavidin magna beads. Radioactive Fe that had been chelated by transferrin was visualized with a phosphoimager after spotting captured protein onto a nitrocellulose membrane. A control experiment was run in parallel in which incubation with biotinylated apotransferrin was omitted. See also Fig. S3. Apo Tf, apotransferrin. All P-values were determined using Student's t-test, unless indicated otherwise.

Journal of Cell Science (2016) 129, 843-853 doi:10.1242/jcs.180356

A study of the intracellular compartments through which apotransferrin transits revealed that, as in the case of holotransferrin, most of the internalized apotransferrin was rapidly localized to early and recycling endosomes (Rab5a- and Rab11a-positive vesicles). Around half (54.4±13%, mean±s.d.) of the apotransferrin-positive vesicles colocalized with clathrin, suggesting a role for clathrin-pit-mediated endocytosis, as well as for alternative pathways of endocytosis. A minor fraction of apotransferrin-carrying vesicles were observed to colocalize with late-endosomal marker Rab7 (Rab7a; 19.2±8.2%) and the lysosomal marker lamp1 (16.2±5.9%), which might represent the fraction destined for degradation (Fig. 4A–E).

To characterize and establish the distinct nature of the GAPDH–apotransferrin recycling process, we characterized the kinetics of its trafficking into cells. The steady-state internal-to-surface ratio of apotransferrin in Fe-loaded CHO-TRVb cells was found to be 0.089±0.065 (mean±s.d.). The internalization rate constant, evaluated by using two complementary methods, gave similar values of 0.26±0.032 min^{-1} (internalization of the apotransferrin ligand; mean±s.d.; Fig. 5A) and 0.24±0.020 min^{-1} (internalization rate of GAPDH receptor; Fig. 5B). This value is much higher than that reported for internalization of holotransferrin through GAPDH in the same cells (Kumar et al., 2012). It is also higher than the value obtained previously for holotransferrin internalization through transferrin receptor protein 1 (TfR1), determined using CHO cells (Johnson et al., 1994). We also obtained comparable recycling rates of 0.18±0.017 min^{-1} and 0.195±0.039 min^{-1} for receptor and ligand, respectively. These values are also distinct from the recycling rates of the holotransferrin GAPDH receptor characterized earlier (Kumar et al., 2012) and from the well-described TfR1 (Johnson et al., 1994). The closely matching values suggest that the internalization and recycling of the two partners (apotransferrin and cell surface GAPDH) are coupled. Finally, we also observed that a small fraction of ligand internalized into cells is slowly degraded over several hours (Fig. 5E).

DISCUSSION

Our results indicate that apotransferrin internalization and recycling is a more rapid phenomenon that is distinct from the well-described recycling process of holotransferrin and its receptor for intracellular Fe delivery. As the temporal consequences of cellular Fe excess are far more deleterious that those of Fe depletion, cells dealing with excess intracellular Fe require rapid sequestration and elimination of the excess ions. To achieve this, swift internalization and recycling of apotransferrin is crucial, especially in cells that do not possess extensive Fe storage capacity (high levels of ferritin).

To maintain optimum availability of Fe (or for that matter any vital resource), living organisms have developed well-orchestrated homeostatic mechanisms to regulate absorption, transport and elimination at the cellular and systemic level. In vertebrates, this involves specific receptor-mediated uptake of Fe-carrier molecules coupled with Fe transporters. GAPDH is known to have a very diverse range of functions and, at least in its roles in the maintenance of Fe homeostasis, it is known to possess higher-order multifunctionality (Boradia et al., 2014a,b). Glycolytic enzymes, expressed in high copy number, would have evolved during the early development of cells. They are ideal candidates for endowment with multiple functions. It is conceivable that evolution of GAPDH as a player in the maintenance of Fe levels could have occurred before specialized transporter molecules (such as ferroportin) evolved along with the appearance of higher developed metazoans with polarized cells lining the alimentary canal.

In summary, our current findings suggest that GAPDH mediates the internalization of apotransferrin to facilitate Fe export through treadmilling of this Fe carrier in and out of cells in a manner reminiscent of the reverse overshot water-wheel, which has been in use since antiquity to pump out water from flooded mines. To date, the movement of transition metal ions out of cells has been considered to be only through transmembrane ion channels, and our current results reveal a totally new dimension to cellular metal ion export and also highlight the higher-order multifunctional nature of GAPDH in the maintenance of cellular Fe homeostasis. A schematic representation of this process is presented in Fig. 6.

MATERIALS AND METHODS

Cell lines, primary cells and materials

The mouse macrophage cell line J774 was procured from European Collection of Authenticated Culture Collections. The CHO-TRVb (derived from CHO cells) cell line, which lacks both TfR1 and transferrin receptor 2 and does not express ferroportin on its surface was kindly provided by Prof. T. McGraw (Weill Medical College of Cornell University, New York, NY; McGraw et al., 1987) and Dr S. Mayor (National Centre for Biological Sciences, Bangalore, India). The NS (mouse fibroblast) cell line was a gift from Prof. A. Takashima (University of Texas Southwestern Medical Center, Dallas, TX; Xu et al., 1995). CHO and THP1 cell lines were obtained from the National Centre for Cell Sciences, Pune, India. THP1 cells were activated through incubation with 12.5 ng/ml of phorbol 12-myristate 13-acetate (PMA) for 24 h. A stable THP1 cell line in which knockdown of total cellular GAPDH (by using GAPDH shRNA lentiviral particles) has been established previously (Sheokand et al., 2013) was used in the study. CHO-TRVb cells were silenced for GAPDH expression (by using GAPDH siRNA), as described previously (Kumar et al., 2012). All primary cells (hepatocytes, bone marrow, spleen macrophages and spleen lymphocytes) were obtained from Sprague Dawley rat or Balb/c mice, as described previously. Cells positive for F4/80 antigen (encoded by *ADGRE1*) were selected as macrophages from the total population of bone marrow and spleen cells by using flow cytometry (Lin et al., 2010). Cells were maintained in RPMI-1640 medium supplemented with 10% fetal calf serum and regularly tested for contamination and purity. All animal handling protocols were as approved by the institutional animal ethics committee. Blood for isolation of human peripheral blood lymphocytes was obtained from normal healthy volunteers with due informed consent and as approved by the statutory CSIR, Institute of Microbial Technology ethics committee as per relevant institutional procedures. Plasmids for expression of Rab5–GFP, Rab7–GFP, clathrin–CFP and lamp1–RFP were kindly provided by Dr Jennifer Lippincott Schwartz (National Institutes of Health, Bethesda, MD). Ferroportin plasmid construct (Fpn-eGFP-N1) was obtained as a gift from Drs Jerry Kaplan and Diane McVey Ward (University of Utah, UT). The plasmid expressing Rab11a–mCherry was a gift from Professor Kazuhisa Nakayama (Kyoto University, Japan).

Cell treatment

For Fe loading, cells were incubated with 100 µM Fe as $FeCl_3$ in complete medium for 24 h, as described previously. Controls were set up in parallel with normal medium. No significant change in viability was observed, as assessed with Trypan Blue, sulforhodamine and propidium iodide assays, as described previously (Sheokand et al., 2014).

Flow cytometry analysis

All flow cytometry experiments were performed essentially as described previously (Raje et al., 2007). Briefly, 2×10^5 cells were stained either with 1 µg of monoclonal antibody against GAPDH (Calbiochem, catalog number CB1001) or 1:100 diluted goat anti-ferroportin antibody (Santa Cruz, catalog number sc-49668), followed by a FITC-conjugated sheep anti-mouse IgG antibody (Sigma-Aldrich, catalog number F6257), FITC-conjugated anti-goat IgG antibody (Santa Cruz, catalog number sc-53800). Macrophages were identified by using APC-conjugated anti-F4/80 antibody (eBioscience, catalog number 17-4801-82). Apotransferrin binding was assessed by using 10 µg apotransferrin conjugated to Alexa-Fluor-647. The incubation buffer for

Journal of Cell Science (2016) 129, 843-853 doi:10.1242/jcs.180356

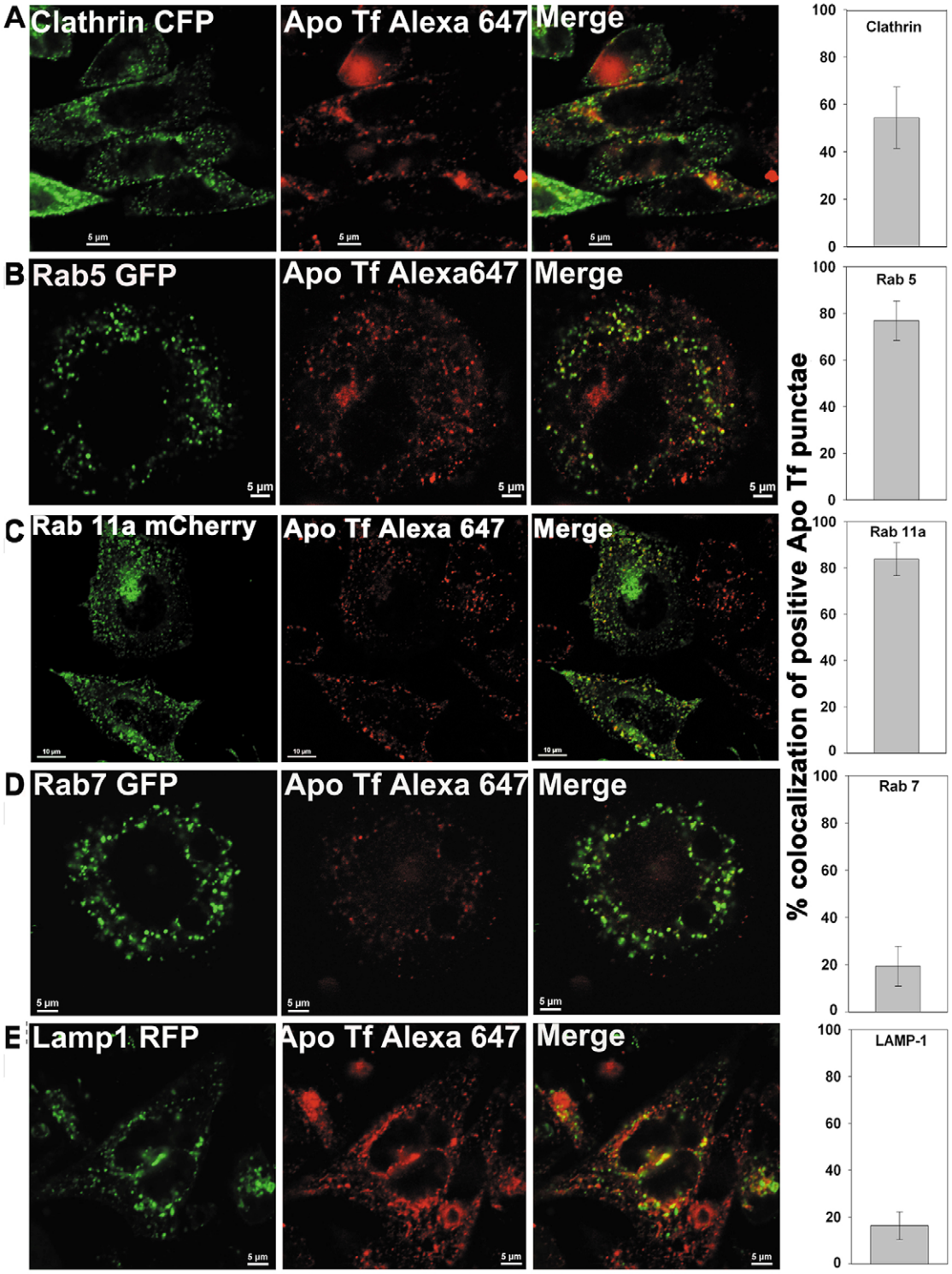

Fig. 4. Intracellular trafficking of apotransferrin. (A–E) Colocalization of apotransferrin–Alexa-Fluor-647 into clathrin–CFP- (A), Rab5–GFP- (B), Rab11a–mCherry- (C), Rab7–GFP- (D) or lamp1–RFP-positive (E) compartments in Fe-loaded CHO-TRVb cells. The bar graph on the right-hand side of each set indicates the percentage colocalization of apotransferrin-containing vesicles with the indicated markers. Data are presented as the percentage of the total number of apotransferrin vesicles colocalized, *n*=10 cells in each case with minimum 50 apotransferrin-positive vesicles in each cell, mean±s.d. Apo Tf, apotransferrin.

all apotransferrin-binding experiments included 100 µM desferrioxamine (DFO) to prevent incorporation of any Fe into apotransferrin (Kawabata et al., 2000; Sheokand et al., 2014). For intracellular staining, cells were fixed with 2% paraformaldehyde and treated with 0.1% saponin before incubation with antibodies. From each sample, 10^4 cells were analyzed using FACS Calibur or FACS Verse flow cytometers (BD Biosciences), and data are presented as mean fluorescence intensity± s.e.m. (MFI±s.e.m.).

Colocalization analysis with confocal microscopy

Fe-loaded cells plated onto glass-bottomed Petri dishes were blocked with 2% BSA in serum-free medium (SFM). For colocalization analysis of internalized

Journal of Cell Science (2016) 129, 843-853 doi:10.1242/jcs.180356

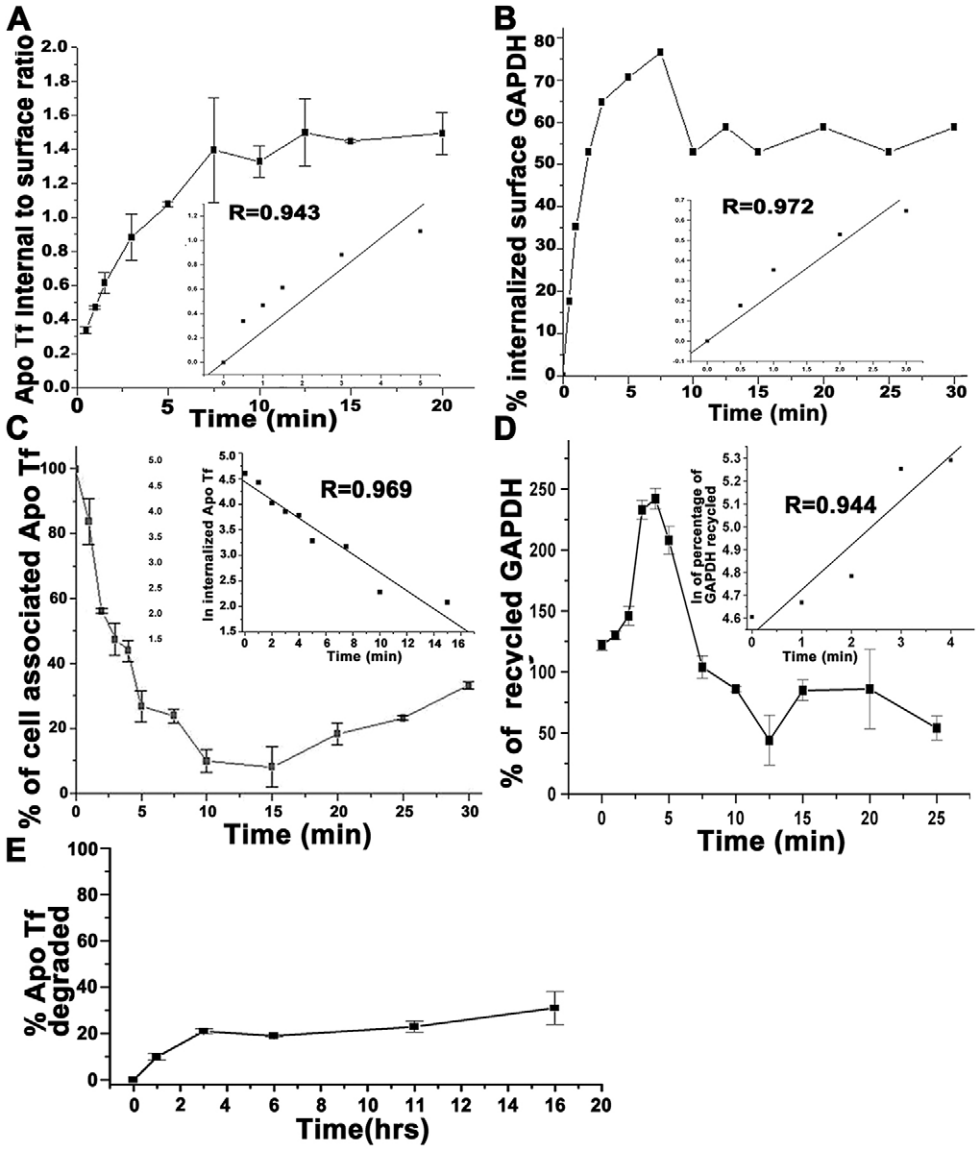

Fig. 5. Kinetics of GAPDH and apotransferrin internalization. (A) Time-dependent internalization of apotransferrin (Apo Tf) into Fe-loaded CHO-TRVb cells; data are plotted as the ratio of intracellular to cell-surface-associated apotransferrin versus time. The internalization rate constant was calculated from the initial linear portion of the curve (inset). (B) Antibody-staining-based analysis of surface GAPDH internalization kinetics; data are plotted as the percentage of the total surface-bound anti-GAPDH antibody that is internalized versus time. The internalization rate constant was calculated from the initial linear portion of the curve (inset). (C) Recycling kinetics of internalized apotransferrin; data are presented as the percentage of the total cell-associated apotransferrin signal versus time. The recycling rate constant of apotransferrin was measured from the initial linear portion of the curve (inset). (D) Antibody-based recycling kinetics of surface GAPDH expressed as percentage of the anti-GAPDH antibody that is recycled versus time. The recycling rate constant was measured from the initial linear portion of the curve (inset). Insets for C,D have the *y*-axis plotted as the natural log of the percentage cell-associated signal versus time. (E) Degradation of internalized apotransferrin. Fe-loaded CHO-TRVb cells were incubated with [^{125}I] apotransferrin at 37°C for 120 min. After extensive washing, cells were incubated in pre-warmed SFM for different time points at 37°C. Culture medium was then precipitated using TCA, and radioactivity in the supernatant (degraded apotransferrin) was measured. The *y*-axis represents degraded transferrin as the percentage of the total apotransferrin internalized. Mean±s.d.

GAPDH and apotransferrin, cells were incubated with 1 µg of monoclonal anti-GAPDH antibody followed by sheep anti-mouse FITC and 10 µg of apotransferrin–Alexa-Fluor-647 at 4°C. Subsequently, cells were shifted to 37°C for 10 min to allow internalization of surface proteins. For colocalization studies of apotransferrin with Rab5, Rab7, Rab11a, clathrin, lamp1 or ferroportin, CHO-TRVb cells plated in glass-bottomed Petri dishes were first transfected with either of Rab5–GFP, Rab7–GFP, Rab11a–mCherry, clathrin–CFP, lamp1–RFP or ferroportin–EGFP plasmids using lipofectamine transfection reagent (Invitrogen) as per the manufacturer's instructions. Subsequently, cells were loaded with Fe for 24 h and allowed to internalize 10 µg of apotransferrin–Alexa-Fluor-647 at 37°C for 5 min. In the case of ferroportin–EGFP-transfected CHO-TRVb cells, the surface GAPDH was first marked with monoclonal anti-GAPDH antibody+anti-mouse Alexa-Fluor-568-conjugated antibody (Invitrogen, catalog number A11061) and the complex was allowed to traffic into cells along with apotransferrin. Finally, cells were washed, fixed in 1% paraformaldehyde and imaged with a Nikon AIR confocal microscope using a 60× objective and 1 airy unit aperture.

Radiolabeling of apotransferrin

Human apotransferrin was procured from Calbiochem and radiolabeled with Na[^{125}I] (Perkin Elmer) using chloramine-T. The specific activity was typically ~200 cpm/ng. Conjugates of apotransferrin with Alexa-Fluor-647, FITC and biotin were prepared exactly as described previously (Sheokand et al., 2013, 2014).

Interaction and internalization of GAPDH–apotransferrin

Internalization of apotransferrin was evaluated by labeling and FACS-based assays. To study the uptake of [^{125}I]apotransferrin, different cell lines were plated onto a 24-well plate (2×10^5 cells/well) and loaded with Fe by incubation in 100 µM $FeCl_3$-supplemented medium for 24 h. Subsequently, the wells were blocked with 2% BSA for 30 min at 4°C, and cells were incubated with 20 µg of [^{125}I]apotransferrin at 37°C for 10 min. Incubation buffer included 100 µM DFO as described above to retain transferrin in the Fe-free form before cellular uptake. Cells were then treated with 0.1% pronase at 4°C for 10 min to remove any residual surface-bound ligand. Finally, samples were lysed with 10% SDS, and internalized apotransferrin was measured using a γ-counter (Perkin Elmer).

Interaction of GAPDH with apotransferrin on the cell surface, as well as in internalized endosomes of CHO-TRVb cells that had been treated with excess Fe, was assessed by co-immunoprecipitation and acceptor photobleaching FRET analysis, as described previously (Boradia et al., 2014a,b). Briefly, Fe-loaded CHO-TRVb or J774 cells were incubated with biotinylated apotransferrin at 4°C to allow surface binding, and the purified membrane fraction was used for co-immunoprecipitation with Streptavidin magna beads® (Pierce). Interaction with GAPDH was confirmed by western blot using monoclonal anti-GAPDH antibody. A control was performed wherein incubation of cells with biotinylated apotransferrin was omitted; as an additional control, membrane from cells incubated in normal medium was also utilized for co-immunoprecipitation. To evaluate the interaction of internalized

Journal of Cell Science (2016) 129, 843-853 doi:10.1242/jcs.180356

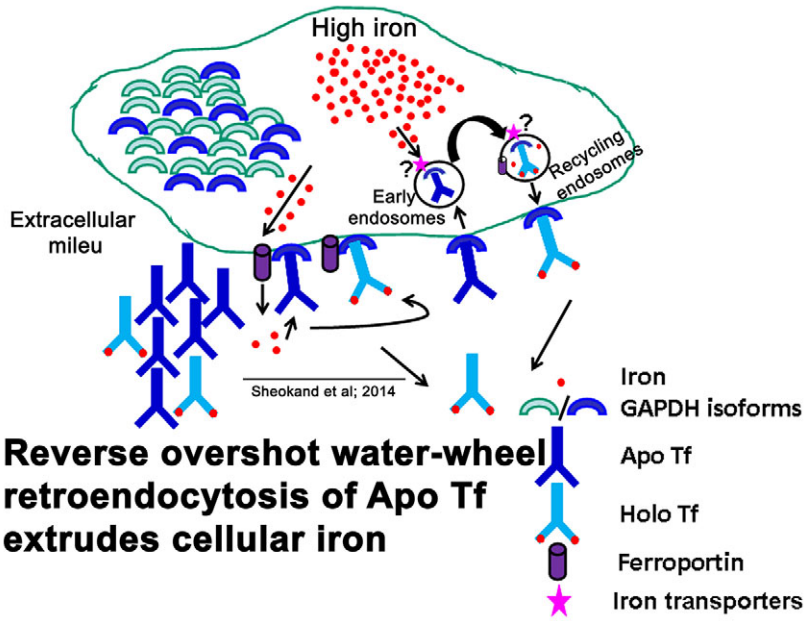

Fig. 6. Schematic representation of apotransferrin recycling through cells, resulting in Fe extrusion.

receptor and ligand after surface binding, cells were incubated at 37°C for 10 min before preparation of the endosomal fraction, which was subjected to co-immunoprecipitation and western blot analysis as above. In the case of acceptor photobleaching experiments, the FRET efficiency was calculated as signal intensity of ($donor_{post\text{-}bleach}$−$donor_{pre\text{-}bleach}$)/$donor_{post\text{-}bleach}$×100 and was compared to a non-specific control where anti-goat IgG Alexa-Fluor-647-conjugated antibody (Invitrogen, catalog number A21246) was substituted for apotransferrin–Alexa-Fluor-647 as the acceptor while keeping anti-GAPDH followed by anti-mouse IgG TRITC-conjugated antibody (Bangalore Genie, catalog number RTC3) as the donor.

Detection of colocalization of cell surface GAPDH and apotransferrin in purified endosomes with immunogold-labeling transmission electron microscopy

To visualize trafficking of apotransferrin along with GAPDH that was originally present on the surface of cells into endosomes, 5×10^7 Fe-treated CHO-TRVb cells were incubated with rabbit anti-GAPDH antibody (Sigma-Aldrich, G9545) or isotype control, followed by anti-rabbit 5-nm-gold-conjugated antibody (Abcam, catalog number ab27240) along with apotransferrin conjugated with 20-nm gold particles. After binding to cell surface GAPDH, the entire complex was allowed to internalize at 37°C for 10 min, and endosomes were isolated as described previously (Raje et al., 2007). Purified endosomes were adsorbed onto carbon-coated nickel grids, negatively stained using 2% phosphotungstic acid+2% uranyl acetate and viewed using a JEOL JEM 2100 transmission electron microscope.

Binding of apotransferrin to cells is saturable

CHO-TRVb cells were cultured on 96-well plates (2×10^4 cells/well) and treated with 100 µM $FeCl_3$. Saturable binding of apotransferrin to cells was assessed by analyzing the capture of biotinylated apotransferrin (which was detected with Streptavidin-conjugated horseradish peroxidase) by cells, essentially as described previously (Kumar et al., 2012). To determine the binding affinity, ligand concentration versus optical density (OD) data were fitted by nonlinear regression for one site specific saturable binding using GraphPad® software.

Fe-release assay using radioactive Fe

This was performed essentially as described previously, different cell types were subjected to Fe loading using $FeCl_3$ in complete medium as above but which had been spiked with 500 nM of [^{55}Fe]Cl_3 (Sheokand et al., 2014). Controls were set up in parallel with complete medium containing only 500 nM of radioactive [^{55}Fe]Cl_3. After 12 h, cells were washed extensively with SFM and incubated with or without 3 mg/ml of apotransferrin at 37°C for 1 h. After the incubation was over, supernatants were collected and analyzed for released radioactive Fe by using liquid scintillation counting.

Colorimetric Fe-release assay

Cells were loaded with Fe by incubation with 100 µM $FeCl_3$ for 24 h. After treatment, the cells were harvested and washed. Aliquots of 1×10^6 cells were incubated in either only SFM or SFM containing 3 mg/ml apotransferrin (in a total volume of 100 µl) at 37°C for 1 h. Subsequently, cells were centrifuged at 500 ***g*** for 5 min to collect supernatant, and the cell pellet was washed three times with neutral buffer (20 mM HEPES, 150 mM NaCl, 5 mM KCl and 1 mM each of $CaCl_2$ and $MgCl_2$). Both cell pellets and respective cell supernatants were digested with 5% HNO_3 at 80°C for 2 h to release Fe. Samples were then concentrated using SpeedVac®, and quantification of Fe levels was performed using a Quantichrome® Fe assay kit (Bioassay Systems), as per the manufacturer's instructions.

Fe accumulation in endosomes

Early endosomes from control as well as Fe-loaded J774 cells (5×10^6/sample) after apotransferrin incubation were purified essentially as above. Each sample was resuspended in 100 µl of PBS, and protein concentration was determined before injection into a Shimadzu AA-6800 atomic absorption spectrometer with a graphite furnace atomizer GFA-EX7. Fe quantification was performed using a standard curve for Fe (Fluka Analytical).

Dependence of cellular Fe export on apotransferrin internalization

CHO-TRVb cells, J774 macrophages and primary hepatocytes, cultured in 24-well plates (2×10^5cells/well), were first loaded with Fe as above and then pre-incubated with 80 µM Dynasore at 37°C for 10 min, in control samples, drug treatment was omitted. Subsequently, cells were assayed for internalization of apotransferrin–Alexa-Fluor-647 as detailed below. To measure Fe extrusion, cells were washed extensively with SFM and incubated with 3 mg/ml of apotransferrin at 37°C for 1 h. After incubation was over, supernatants were collected and analyzed for released radioactive Fe by using liquid scintillation counting. In addition, apotransferrin internalization and Fe extrusion was also evaluated in CHO-TRVb cells utilizing a panel of pharmacological inhibitors of endocytosis, as described earlier (Kumar et al., 2012).

Sequestration of Fe into apotransferrin

CHO-TRVb cells were cultured in 24-well plates (2×10^5 cells/well) and subjected to radioactive-Fe loading, as described above. Cells were then

incubated with 0.5 mg/ml biotinylated apotransferrin, which was allowed to recycle between the cell surface and cytosol at 37°C for 1 h, at which time cell lysate was prepared as before, and separately, the culture supernatant from each sample was collected. Biotinylated apotransferrin was immunoprecipitated from the cell-free supernatant as well as from cell lysates using Streptavidin magna beads® (Pierce) and blotted onto nitrocellulose membrane. Radioactive Fe that had been chelated by transferrin was visualized in a phosphoimager (Fujifilm FLA-9000) after spotting captured protein onto a nitrocellulose membrane. A control experiment was run in parallel where incubation with biotinylated apotransferrin was omitted.

Internalization, recycling and degradation characteristics and kinetics of apotransferrin

Internalization of apotransferrin, rate constant of internalization, surface-to-internal ratio at steady state, recycling of the internalized GAPDH receptor (and associated apotransferrin ligand), degradation of internalized ligand and the effect of a diverse panel of endocytosis inhibitors on apotransferrin trafficking into Fe-loaded CHO-TRVb cells were evaluated exactly as described previously (Kumar et al., 2012; Sheokand et al., 2013). The effect of 80 µM Dynasore®, obtained from Sigma-Aldrich, was additionally studied using J774 macrophages, CHO-TRVb cells and primary hepatocytes. To study the degradation of internalized apotransferrin, Fe-loaded CHO-TRVb cells were incubated with [^{125}I]-apotransferrin at 37°C for 120 min. After extensive washing, cells were incubated in pre-warmed SFM for different time points at 37°C. Culture medium was then precipitated using trichloroacetic acid (TCA), and radioactivity in the supernatant (degraded apotransferrin) was measured.

Specificity, pronase sensitivity and saturability of cellular apotransferrin uptake

Fe-loaded CHO-TRVb cells were incubated with apotransferrin–AlexaFluor-647 at 37°C for 10 min, alone or in the presence of 200 times as much unlabeled ligand. After washing with SFM, the cells were treated with 0.1% pronase to remove any residual surface-bound ligand (Walseng et al., 2008). Internalized apotransferrin was then evaluated by using flow cytometry. To check if trafficking into cells is dependent upon any surface-localized proteins, cells were first pre-treated with 0.1% pronase for 2 min at 4°C to digest native surface proteins and then processed for analysis of ligand internalization as above. To evaluate if the uptake is a saturable process, a concentration-dependent internalization assay was performed, essentially as described previously (Kumar et al., 2012).

Statistical analysis

All statistical analysis was performed using Student's unpaired *t*-test.

Acknowledgements

Mr. Anil Theophilus, Mr. Randeep Sharma and Dr Subash Pawar are acknowledged for technical assistance. This is CISR-IMTECH Communication number 095/2014.

Competing interests

The authors declare no competing or financial interests.

Author contributions

M.R. and C.I.R. conceived the studies, designed the experiments, arranged funding, analyzed the data and wrote the manuscript. N.S. and H.M. designed and performed the FACS, co-immunoprecipitation, microscopy and Fe-release experiments, performed preliminary data analysis and prepared the primary draft of the manuscript. N.S. and A.S.C. performed colocalization experiments. V.B. prepared the plasmids for transfections. A.S.C., M.K., S.C. and A.P. all contributed in the FACS and Fe-exodus studies.

Funding

N.S. was recipient of a research fellowship from Council for Scientific and Industrial Research (CSIR); H.M. and S.C. received fellowships from University Grants Commission, India. V.M.B. received a research fellowship from National Institute of Pharmaceutical Education and Research, Sahibzada Ajit Singh Nagar. A.S.C. and A.P. received fellowships from the Department of Biotechnology, India. M.K. was the recipient of a project assistantship from CSIR. The financial support of CSIR and Department Of Science & Technology is acknowledged.

Supplementary information

Supplementary information available online at
http://jcs.biologists.org/lookup/suppl/doi:10.1242/jcs.180356/-/DC1

References

Abboud, S. and Haile, D. J. (2000). A novel mammalian iron-regulated protein involved in intracellular iron metabolism. *J. Biol. Chem.* **275**, 19906-19912.

Azuma, Y., Takada, M., Shin, H.-W., Kioka, N., Nakayama, K. and Ueda, K. (2009). Retroendocytosis pathway of ABCA1/apoA-I contributes to HDL formation. *Genes Cells* **14**, 191-204.

Boradia, V. M., Malhotra, H., Thakkar, J. S., Tillu, V. A., Vuppala, B., Patil, P., Sheokand, N., Sharma, P., Chauhan, A. S., Raje, M. (2014a). Mycobacterium tuberculosis acquires iron by cell-surface sequestration and internalization of human holo-transferrin. *Nat. Commun.* **5**, 4730.

Boradia, V. M., Raje, M. and Raje, C. I. (2014b). Protein moonlighting in iron metabolism: glyceraldehyde-3-phosphate dehydrogenase (GAPDH). *Biochem. Soc. Trans.* **42**, 1796-1801.

Canonne-Hergaux, F., Donovan, A., Delaby, C., Wang, H.-J. and Gros, P. (2006). Comparative studies of duodenal and macrophage ferroportin proteins. *Am. J. Physiol. Gastrointest. Liver Physiol.* **290**, G156-G163.

D'Anna, M. C., Veuthey, T. V. and Roque, M. E. (2009). Immunolocalization of ferroportin in healthy and anemic mice. *J. Histochem. Cytochem.* **57**, 9-16.

De Domenico, I., Ward, D. M., Musci, G. and Kaplan, J. (2007). Evidence for the multimeric structure of ferroportin. *Blood* **109**, 2205-2209.

Delaby, C., Pilard, N., Gonçalves, A. S., Beaumont, C. and Canonne-Hergaux, F. (2005). Presence of the iron exporter ferroportin at the plasma membrane of macrophages is enhanced by iron loading and down-regulated by hepcidin. *Blood* **106**, 3979-3984.

Donovan, A., Lima, C. A., Pinkus, J. L., Pinkus, G. S., Zon, L. I., Robine, S. and Andrews, N. C. (2005). The iron exporter ferroportin/Slc40a1 is essential for iron homeostasis. *Cell Metab.* **1**, 191-200.

Donovan, A., Roy, C. N. and Andrews, N. C. (2006). The ins and outs of iron homeostasis. *Physiology* **21**, 115-123.

Hentze, M. W., Muckenthaler, M. U. and Andrews, N. C. (2004). Balancing acts: molecular control of mammalian iron metabolism. *Cell* **117**, 285-297.

Johnson, L. S., Presley, J. F., Park, J. C. and McGraw, T. E. (1994). Slowed receptor trafficking in mutant CHO lines of the End1 and End2 complementation groups. *J. Cell. Physiol.* **158**, 29-38.

Kawabata, H., Germain, R. S., Vuong, P. T., Nakamaki, T., Said, J. W. and Koeffler, H. P. (2000). Transferrin receptor 2-α supports cell growth both in iron-chelated cultured cells and in vivo. *J. Biol. Chem.* **275**, 16618-16625.

Kumar, S., Sheokand, N., Mhadeshwar, M. A., Raje, C. I. and Raje, M. (2012). Characterization of glyceraldehyde-3-phosphate dehydrogenase as a novel transferrin receptor. *Int. J. Biochem. Cell Biol.* **44**, 189-199.

Le Gac, G., Ka, C., Joubrel, R., Gourlaouen, I., Lehn, P., Mornon, J.-P., Férec, C. and Callebaut, I. (2013). Structure-function analysis of the human ferroportin iron exporter (SLC40A1): effect of hemochromatosis type 4 disease mutations and identification of critical residues. *Hum. Mutat.* **34**, 1371-1380.

Leong, W.-I. and Lönnerdal, B. (2005). Iron transporters in rat mammary gland: effects of different stages of lactation and maternal iron status. *Am. J. Clin. Nutr.* **81**, 445-453.

Lin, H.-H., Stacey, M., Stein-Streilein, J. and Gordon, S. (2010). F4/80: the macrophage-specific adhesion-GPCR and its role in immunoregulation. In *Adhesion-GPCRs*, pp. 149-156. Springer.

Linder, M. C. (2013). Mobilization of stored iron in mammals: a review. *Nutrients* **5**, 4022-4050.

Linder, M. C., Moriya, M., Whon, A., Kassa, A. and Gilley, C. (2006). Vesicular transport of Fe and interaction with other metal ions in polarized Caco2 Cell monolayers. *Biol. Res.* **39**, 143-156.

Ludwiczek, S., Theurl, I., Muckenthaler, M. U., Jakab, M., Mair, S. M., Theurl, M., Kiss, J., Paulmichl, M., Hentze, M. W., Ritter, M. et al. (2007). Ca2+ channel blockers reverse iron overload by a new mechanism via divalent metal transporter-1. *Nat. Med.* **13**, 448-454.

Ma, Y., Specian, R. D., Yeh, K.-Y., Yeh, M., Rodriguez-Paris, J. and Glass, J. (2002). The transcytosis of divalent metal transporter 1 and apotransferrin during iron uptake in intestinal epithelium. *Am. J. Physiol. Gastrointest. Liver Physiol.* **283**, G965-G974.

McGraw, T. E., Greenfield, L. and Maxfield, F. R. (1987). Functional expression of the human transferrin receptor cDNA in Chinese hamster ovary cells deficient in endogenous transferrin receptor. *J. Cell Biol.* **105**, 207-214.

McKie, A. T., Marciani, P., Rolfs, A., Brennan, K., Wehr, K., Barrow, D., Miret, S., Bomford, A., Peters, T. J., Farzaneh, F. et al. (2000). A novel duodenal iron-regulated transporter, IREG1, implicated in the basolateral transfer of iron to the circulation. *Mol. Cell* **5**, 299-309.

Moriya, M. and Linder, M. C. (2006). Vesicular transport and apotransferrin in intestinal iron absorption, as shown in the Caco-2 cell model. *Am. J. Physiol. Gastrointest. Liver Physiol.* **290**, G301-G309.

Nemeth, E., Tuttle, M. S., Powelson, J., Vaughn, M. B., Donovan, A., Ward, D. M., Ganz, T. and Kaplan, J. (2004). Hepcidin regulates cellular iron efflux by binding to ferroportin and inducing its internalization. *Science* **306**, 2090-2093.

Pagler, T. A., Rhode, S., Neuhofer, A., Laggner, H., Strobl, W., Hinterndorfer, C., Volf, I., Pavelka, M., Eckhardt, E. R. M., van der Westhuyzen, D. R. et al. (2006). SR-BI-mediated high density lipoprotein (HDL) endocytosis leads to HDL resecretion facilitating cholesterol efflux. *J. Biol. Chem.* **281**, 11193-11204.

Raje, C. I., Kumar, S., Harle, A., Nanda, J. S. and Raje, M. (2007). The macrophage cell surface glyceraldehyde-3-phosphate dehydrogenase is a novel transferrin receptor. *J. Biol. Chem.* **282**, 3252-3261.

Ramey, G., Deschemin, J.-C., Durel, B., Canonne-Hergaux, F., Nicolas, G. and Vaulont, S. (2010). Hepcidin targets ferroportin for degradation in hepatocytes. *Haematologica* **95**, 501-504.

Röhrl, C. and Stangl, H. (2013). HDL endocytosis and resecretion. *Biochim. Biophys. Acta* **1831**, 1626-1633.

Ross, S. L., Tran, L., Winters, A., Lee, K.-J., Plewa, C., Foltz, I., King, C., Miranda, L. P., Allen, J., Beckman, H. et al. (2012). Molecular mechanism of hepcidin-mediated ferroportin internalization requires ferroportin lysines, not tyrosines or JAK-STAT. *Cell Metab.* **15**, 905-917.

Sheokand, N., Kumar, S., Malhotra, H., Tillu, V., Raje, C. I. and Raje, M. (2013). Secreted glyceraldehye-3-phosphate dehydrogenase is a multifunctional autocrine transferrin receptor for cellular iron acquisition. *Biochim. Biophys. Acta* **1830**, 3816-3827.

Sheokand, N., Malhotra, H., Kumar, S., Tillu, V. A., Chauhan, A. S., Raje, C. I. and Raje, M. (2014). Moonlighting cell-surface GAPDH recruits apotransferrin to effect iron egress from mammalian cells. *J. Cell Sci.* **127**, 4279-4291.

Soe-Lin, S., Apte, S. S., Andriopoulos, B., Andrews, M. C., Schranzhofer, M., Kahawita, T., Garcia-Santos, D. and Ponka, P. (2009). Nramp1 promotes efficient macrophage recycling of iron following erythrophagocytosis in vivo. *Proc. Natl. Acad. Sci. USA* **106**, 5960-5965.

Soe-Lin, S., Apte, S. S., Mikhael, M. R., Kayembe, L. K., Nie, G. and Ponka, P. (2010). Both Nramp1 and DMT1 are necessary for efficient macrophage iron recycling. *Exp. Hematol.* **38**, 609-617.

Steil, G. M., Ader, M., Moore, D. M., Rebrin, K. and Bergman, R. N. (1996). Transendothelial insulin transport is not saturable in vivo. No evidence for a receptor-mediated process. *J. Clin. Invest.* **97**, 1497-1503.

Walseng, E., Bakke, O. and Roche, P. A. (2008). Major histocompatibility complex class II-peptide complexes internalize using a clathrin- and dynamin-independent endocytosis pathway. *J. Biol. Chem.* **283**, 14717-14727.

Ward, D. M. and Kaplan, J. (2012). Ferroportin-mediated iron transport: expression and regulation. *Biochim. Biophys. Acta* **1823**, 1426-1433.

Xu, S., Ariizumi, K., Edelbaum, D., Bergstresser, P. R. and Takashima, A. (1995). Cytokine-dependent regulation of growth and maturation in murine epidermal dendritic cell lines. *Eur. J. Immunol.* **25**, 1018-1024.

Zhang, Z., Zhang, F., An, P., Guo, X., Shen, Y., Tao, Y., Wu, Q., Zhang, Y., Yu, Y., Ning, B. et al. (2011). Ferroportin1 deficiency in mouse macrophages impairs iron homeostasis and inflammatory responses. *Blood* **118**, 1912-1922.